*Visual Neuroscience* (2005), **22**, 859–871. Printed in the USA.

DOI: 10.1017/S0952523805226147

# Homotypic constraints dominate positioning of on- and off-center beta retinal ganglion cells

STEPHEN J. EGLEN,[1] PETER J. DIGGLE,[2] AND JOHN B. TROY[3]

[1]Department for Applied Mathematics and Theoretical Physics, University of Cambridge, Cambridge UK
[2]Department of Mathematics and Statistics, Lancaster University, Lancaster, UK
[3]Biomedical Engineering Department, Northwestern University, Evanston, Illinois

(RECEIVED June 10, 2005; ACCEPTED August 11, 2005)

**Abstract**

Beta retinal ganglion cells (RGCs) of the cat are classified as either on-center or off-center, according to their response to light. The cell bodies of these on- and off-center RGCs are spatially distributed into regular patterns, known as retinal mosaics. In this paper, we investigate the nature of spatial dependencies between the positioning of on- and off-center RGCs by analysing maps of RGCs and simulating these patterns. We introduce principled approaches to parameter estimation, along with likelihood-based techniques to evaluate different hypotheses. Spatial constraints between cells within-type and between-type are assumed to be controlled by two univariate interaction functions and one bivariate interaction function. By making different assumptions on the shape of the bivariate interaction function, we can compare the hypothesis of statistical independence against the alternative hypothesis of functional independence, where interactions between type are limited to preventing somal overlap. Our findings suggest that the mosaics of on- and off-center beta RGCs are likely to be generated assuming functional independence between the two types. By contrast, allowing a more general form of bivariate interaction function did not improve the likelihood of generating the observed maps. On- and off-center beta RGCs are therefore likely to be positioned subject only to homotypic constraints and the physical constraint that no two somas of opposite type can occupy the same position.

**Keywords:** Beta retinal ganglion cells, Retinal mosaics, Functional independence, Statistical independence, PIPP model

## Introduction

Beta (X) retinal ganglion cells (RGCs) are divided into on-center and off-center types, depending on their response to light (Kuffler, 1953; Enroth-Cugell & Robson, 1966; Boycott & Wässle, 1974). This physiological distinction of beta ganglion cells is mirrored by an anatomical distinction: the dendrites of adult on-center cells ramify mostly in the inner part of the inner plexiform layer (IPL), whereas off-center dendrites are mostly found in the outer part of the IPL (Famiglietti, Jr. & Kolb, 1976; Nelson et al., 1978). The cell bodies of each type form a regular pattern, termed "retinal mosaics" due to the way the cell bodies and dendrites tile the retinal surface. An important question in developmental neuroscience is to understand how the mosaics of on- and off-center RGCs emerge during development. Two possibilities for their development are:

1. A neuronal precursor cell has the potential to become either an on- or off-center beta RGC. The choice of one precursor cell to become, for example an on-center RGC, may inhibit neighboring precursor cells from also adopting the on-center type, driving them instead to become off-center cells. These interactions between cells may be influenced by neuronal activity (Bodnarenko & Chalupa, 1993).
2. The decision of a cell to become on- or off-center may be driven by intrinsic factors, rather than heterotypic interactions. An individual postmitotic cell may therefore be destined to become an on-center beta RGC, rather than passing through a phase when the cell is capable of becoming either an on- or off-center RGC.

By studying the mosaics of on-and off-center beta cells at adulthood, we hope to be able to infer which of the above hypotheses is more likely. In particular, if the mosaics of on- and off-center cells are independent of each other at maturity, one would imagine that the two types of cell develop independently. Conversely, if there are spatial dependencies in the positioning of the two cell types at adulthood, this may be the result of some heterotypic interactions during development.

Address correspondence and reprint requests to: Stephen J. Eglen, Department for Applied Mathematics and Theoretical Physics, University of Cambridge, Wilberforce Road, Cambridge CB3 OWA, UK. E-mail: S.J.Eglen@damtp.cam.ac.uk

Various statistical methods have been developed to test if a sample of cell bodies is regularly distributed (Wässle & Riemann, 1978; Cook, 1996). Rodieck (1991) introduced the density recovery profile (DRP), which calculates the average number of cells as a function of distance surrounding a cell in the array. Counts of cells are plotted as a histogram showing the average density of cells within a given range of distances, with the width of each histogram bin typically 5–10 $\mu$m (Fig. 1). A flat histogram indicates cells are positioned randomly with respect to each other. However, a reduced density (also known as a dip) in the left part of the histogram indicates the cells are regularly arranged. Such correlation techniques have been used previously in other areas of spatial statistics (Ripley, 1976, 1977), but Rodieck's approach has been subsequently adopted for many studies of retinal organization (e.g. Cook, 1996; Kouyama & Marshak, 1997; Rockhill et al., 2000).

This DRP method was extended to test for spatial dependencies between two types of retinal cell (Rodieck, 1991), called the cross DRP here. This method was used to investigate the spatial relationship between those cholinergic amacrine cells found in the inner nuclear layer and those found in the ganglion cell layer (Rodieck & Marshak, 1992). No dips were found in the cross DRPs of the cholinergic amacrines from macaque and human retinas, and thus it was concluded that the two arrays of amacrines, found in different layers of the retina, were spatially independent of each other. This result confirmed earlier analysis by Diggle (1986) also using second-order methods. The cross DRP has subsequently been applied to several different pairs of retinal cell, leading to the general conclusion that there are no spatial dependencies between different types of retinal cell (Rockhill et al., 2000; Cook & Podugolnikova, 2001). Only a few exceptions to this conclusion have been reported (Kouyama & Marshak, 1997; Ahnelt et al., 2000; Zhan & Troy, 2000; Diggle et al., 2005). Additionally, cross-correlation techniques (Diggle, 1986) were used to demonstrate that dopaminergic amacrine cells found in two different layers of ferret retina form a single functional population (Eglen et al., 2003).

One problem of the cross DRP method occurs when the somas of the two cell types being compared are co-planar. Since the somas are of finite size, there is a lower bound on the minimal distance that can be observed between cells. This necessarily results in a dip in the first bins of the cross DRP (Fig. 1) and thus the locations of the two cell types must be *statistically dependent*. Many would regard this as a trivial dependence. In this paper, we introduce a new model-based approach for testing independence between cell types. We test for statistical dependence (a useful means to check that sample size is adequate) and for dependence beyond that due simply to the restriction forced by distributing finite-sized elements in the same plane. Following the statistical formalism previously developed (Diggle et al., 2005), we call such a dependence *functional dependence*.

Here we apply our models to the important problem of addressing whether the on- and off-center beta RGCs are statistically and/or functionally independent of each other. We use the pairwise interaction point process (PIPP) model (Ripley, 1976, 1977) to replicate distributions of retinal cells, and use likelihood-based methods of inference for evaluating different hypotheses regarding interactions between the on- and off-center RGCs. These likelihood-based inference methods have recently been described elsewhere in detail (Diggle et al., 2005).

## Materials and methods

### *Data sets*

The bivariate data we have analyzed in this paper are shown in Fig. 2. These fields will be referred to by their keys: W81S1 and M623. Field W81S1 was created by digitizing the map shown in Fig. 6 of Wässle et al. (1981*a*). Field M623 was taken from a previous study (Zhan & Troy, 2000). These two are the only published fields to our knowledge that are sufficiently spatially homogeneous and contain enough cells for our analysis.

### *Confirmation of statistical dependence*

Since the somas of on- and off-center RGCs are both located in the ganglion cell layer, then strictly the on- and off-center cells cannot be statistically independent. A failure to reject statistical independence for these mosaics would indicate that we have insufficient data to make inferences about the nature of the dependence between the two types of cell. To test for statistical independence between two fields, we have followed the approach of Diggle

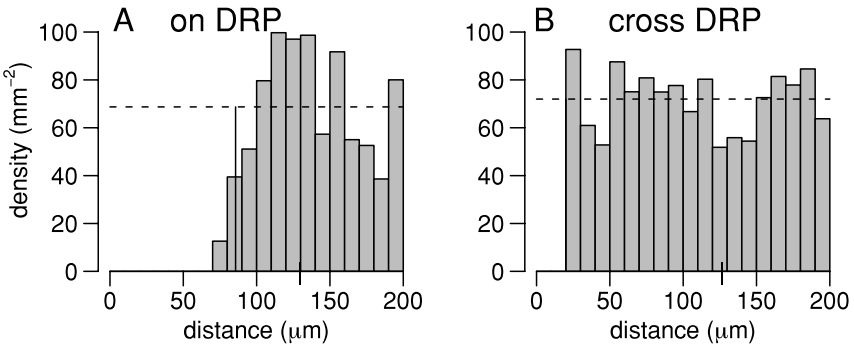


**Fig. 1.** Example density recovery profiles of beta RGCs. Two beta cell arrays (M623 and W81S1) were studied. (A) DRP of the M623 on-center cells. (B) Cross DRP of the M623 on- versus off-center cells. In each plot, the dotted horizontal line shows the expected profile if the points were randomly arranged with respect to cells of same type (A) and cells of opposite type (B). The vertical line indicates the effective radius of the central dip (Rodieck, 1991). In A, the dip in the profile out to around 100 $\mu$m indicates that the cells are regularly arranged. The dotted line indicates the density of the on-center cells. In B, the dip out to 20 $\mu$m could indicate either some form of spatial dependency between the on- and off-center cells or it could just reflect steric hindrance. Here, the dotted line indicates the geometric mean of the on-center and off-center densities (Rodieck, 1991). The DRPs for the W81S1 dataset are qualitatively similar, and so are not shown here.

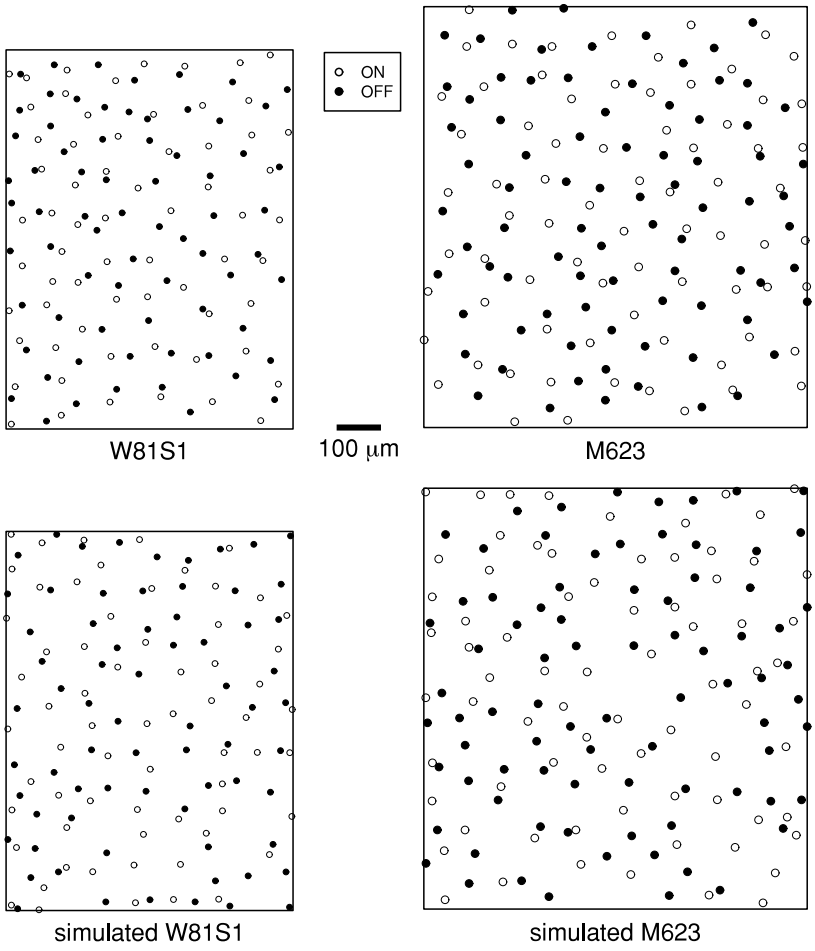


**Fig. 2.** Mosaics of cat beta RGC somas used for this study. Both maps drawn to the same scale with cell body diameter assumed to be 15 $\mu$m (W81S1) and 20 $\mu$m (M623). Rectangles surrounding each plot indicate the sampling window used. Beneath each field is an example simulation of the field using the models developed in this paper (see later).

(1986), which in turn uses Ripley's (1976) $K$ function (we define $K$ functions in a later section). In this case, each simulation consists of toroidally shifting all on-center cells by the same random vector (Lotwick & Silverman, 1982) and computing $K_{12}$ between the shifted on-center cells and the original off-center cells. We then compute the discrepancy between $K_{12}(t)$ and the expected value for no interaction:

$$T^i = \int_0^{150\,\mu\mathrm{m}} (\sqrt{K_{12}^i(t)} - \sqrt{\pi t^2})^2 \, \mathrm{d}t. \tag{1}$$

Here $i = 1$ is for the real $K_{12}$ function, and $i = 2 \ldots s + 1$ are for the $K_{12}$ functions from $s$ randomly shifted data sets. The number of simulations, $s$, for each test is 999. If the rank of $T_1$ among $T$ is less than $[0.05 \times (1 + s)]$, we can reject statistical independence at the $P = 0.05$ level. The upper limit of integration used here, 150 $\mu$m, was chosen based on the heuristic that the limit should typically be no more than $\frac{1}{4}$ the length of the shorter side of the rectangular sampling area, as estimates of $K$ become more variable with increasing distances (Diggle, 2002).

### *PIPP model*

The pairwise interaction point-process (PIPP) model is a flexible means to generate spatial distributions of points (Diggle, 2002). Interactions between pairs of cells are controlled by an interaction function, $h(u)$, where $u$ is the distance between a pair of cells; the joint probability density of a configuration of $n$ cells is proportional to the product of values of $h(u)$ calculated for all pairs of cells.

The simplest form of interaction function is $h(u) = 1$, which implies that there is no spatial dependency between cells. Patterns generated by such an interaction function exhibit complete spatial randomness (CSR). The following interaction function is known as simple inhibition since it just ensures that no two cells are less than the threshold distance $\delta$ apart:

$$\text{simple inhibition: } h(u) = \begin{cases} 0 & : \quad u < \delta \\ 1 & : \quad u \geq \delta \end{cases}. \tag{2}$$

In the special case where $\delta$ is set to the soma diameter, simple inhibition implements the constraint that no two cell bodies can overlap. For a given density of cells, the larger the value of $\delta$, the more regular the pattern. Since the interaction function is circularly symmetric, triangular (but not rectangular) lattices can be generated by this model. This is appealing since previous work has shown that jittered triangular lattices can also replicate beta RGC maps (Zhan & Troy, 2000).

In this paper, we use a parametric form of $h(u;\theta)$, where $\theta = (\delta, \phi, \alpha)$, that is suitably flexible to generate a wide range of spatial patterns:

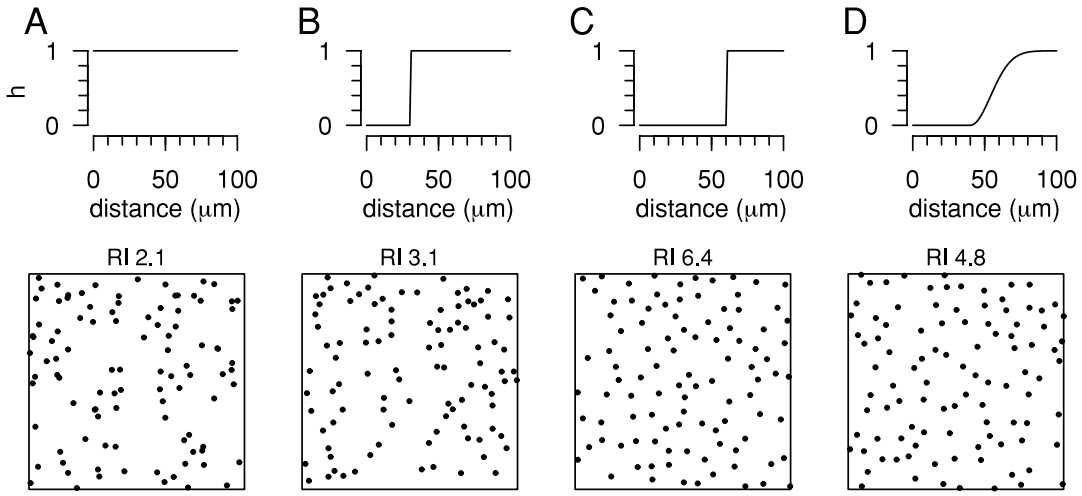


**Fig. 3.** Examples of spatial point patterns created by various interaction functions. In each plot, we show the interaction function above and a simulated data set below ($n = 100$ points in a sample area of size 1000 $\mu$m $\times$ 1000 $\mu$m; cell bodies drawn assuming 10-$\mu$m radius). The regularity index ($RI$) of each spatial pattern is given above each plot. (A) Complete spatial randomness (CSR); points can be arbitrarily close or distant from each other. (B) Simple inhibition ($\delta = 30$ $\mu$m). (C) Simple inhibition ($\delta = 60$ $\mu$m). (D) Sigmoidal interaction function from equation 3 with ($\alpha = 2, \phi = 20$ $\mu$m, $\delta = 40$ $\mu$m).

$$h(u;\theta) = \begin{cases} 0 & : \quad u \leq \delta \\ 1 - \exp[-\{(u-\delta)/\phi\}^{\alpha}] & : \quad u > \delta \end{cases}. \tag{3}$$

The parameter $\delta$ controls when the interaction function first becomes nonzero; $\phi$ determines the range of $u$ over which the interaction function changes from $h(u) = 0$ to $h(u) = 1$. As $\alpha$ increases, the slope of the sigmoidal function increases. By varying the parameters of this function, we can create a wide range of sigmoidal interaction functions, of varying extent and steepness. Fig. 3 shows examples of different interaction functions and spatial patterns generated by them.

We can extend the PIPP model from handling univariate datasets to bivariate datasets by introducing three functions, $h_{11}, h_{22}, h_{12}$, which describe, respectively, the interactions among on-center cells, among off-center cells, and between the on- and off-center cells.

A sufficient condition for the PIPP model to be well-defined is that the interaction functions should be restricted to take values between 0 and 1. In the univariate case, this restriction implies that the PIPP model can generate a wide range of patterns exhibiting varying degrees of spatial regularity, from lattice-like patterns at one extreme to complete spatial randomness at the other, but cannot generate aggregated patterns. In the bivariate case, as discussed by Diggle et al. (2005), the model can also generate spatially aggregated patterns according to the interplay amongst all three interaction functions.

To test for functional dependence between on- and off-center cells, we can use the null hypothesis of simple inhibition with $\delta_{12}$ set to the average soma diameter to describe the $h_{12}$ interaction. Simple inhibition for $h_{12}$ can then be compared against the general bivariate model, where $h_{12}(u) = h(u;\theta_{12})$, that is, where we allow the more flexible form of interaction function as specified in eqn. (3).

*2.3.1. Simulating PIPP models*

Given the functions $h_{11}(u), h_{22}(u), h_{12}(u)$, we can simulate a bivariate spatial pattern of $n_1$ on-center cells and $n_2$ off-center cells using a birth and death procedure (Ripley, 1977, 1979) as outlined below. The position of the $i$th type 1 cell is given by the two-dimensional (2D) vector $\mathbf{x}_{1i}$, and all cells are assumed to be positioned within the sampling window $A$ with area $|A|$.

*Initial conditions*: $n_1$ on-center cells and $n_2$ off-center cells are positioned randomly within the simulated array. Alternatively, we can set the initial positions in the simulation to be the same as the real positions; this helps reduce number of iterations needed for convergence.

*Birth-and-death step*: One of the on-center cells, cell $i$, is deleted from the array. A new trial position $\mathbf{x}_{1i}$ is generated at random to replace cell $i$; that position is accepted with probability $p$:

$$p = \prod_{j=1,\, j\neq i}^{n_1} h_{11}(\|\mathbf{x}_{1i} - \mathbf{x}_{1j}\|) \prod_{j=1}^{n_2} h_{12}(\|\mathbf{x}_{1i} - \mathbf{x}_{2j}\|). \tag{4}$$

The position of each on-center cell is updated in the same fashion. Once all the on-center cells have been moved once, the off-center cells are then moved, where this time the probability of acceptance for a trial position $\mathbf{x}_{2i}$ is

$$p = \prod_{j=1,\, j\neq i}^{n_2} h_{22}(\|\mathbf{x}_{2i} - \mathbf{x}_{2j}\|) \prod_{j=1}^{n_1} h_{12}(\|\mathbf{x}_{2i} - \mathbf{x}_{1j}\|). \tag{5}$$

One sweep of the algorithm corresponds to moving all cells once. Usually, around ten sweeps are sufficient for convergence of the cell positions to a stable pattern (Ripley, 1979). The order in which cells are moved within a sweep is not important as long as enough sweeps are performed and the algorithm ensures that all cells are visited equally often in the long run; two strategies which meet this requirement are to visit each cell in turn, or to visit cells randomly. When simulating the beta RGC maps, $n_1$ is set to the number of on-center cells, and $n_2$ is the number of off-center cells. Furthermore, the size of the simulated field is the same as the real field so that our simulated maps are of the same density.

*Nonparametric estimation of interaction functions*

Given a spatial point pattern, we can get a nonparametric estimate of the interaction function using a version of maximum pseudolikelihood estimation (Besag, 1978) in conjunction with a piece-wise constant specification of $h(u)$, as suggested in Heikkinen and Penttinen (1999) and in Baddeley & Turner (2000) and implemented in the "spatstat" package for R (Baddeley & Turner, 2005). Once the nonparametric estimate of $h(u)$ for a dataset has been computed, it can be used directly to simulate new fields. This provides a quick way for simulating new fields with similar spatial properties to the real dataset.

*Parametric fits to interaction functions*

Previous work in retinal mosaics has mostly used *ad-hoc* searching of parameter space to find the model parameters that best fit the data. In this paper, we use a nonlinear least-squares method to estimate univariate parameters within the model specified by eqn. (3). Least-squares fitting was performed in R using the optim function. For the univariate fits, we estimated the parameters $\alpha$ and $\phi$ in eqn. (3) but, rather than estimating $\delta$, we constrained it to be 15 $\mu$m. This is our estimate of the lower bound of soma diameter for beta RGCs, considering data from the current maps and prior literature (Stein et al., 1996; Zhan, 1996; Zhan & Troy, 2000).

For fitting the bivariate functional independence model, we use a Monte Carlo likelihood ratio method as follows [a more detailed description is given in (Diggle et al., 2005)].

The functional independence model includes a simple inhibitory interaction function $h_{12}(u)$ as specified by eqn. (2), thereby adding to the model a single parameter $\delta_{12}$, the minimum permissible distance between two cells of opposite types. For any value of $\delta_{12}$, we let $R(\delta_{12})$ denote twice the Monte Carlo log-likelihood ratio between the specified value of $\delta_{12}$ and the value $\delta_{12} = 0$ corresponding to statistical independence. The Monte Carlo maximum likelihood estimate of $\delta_{12}$ is the value $\hat{\delta}_{12}$ which maximises $R(\delta_{12})$. To test the hypothesis that $\delta_{12} = 0$, that is, statistical independence, against the more general alternative of functional independence we then compare $R(\hat{\delta}_{12})$ with the critical value of the chi-squared distribution on 1 degree of freedom, but using twice the required significance level because the null hypothesis corresponds to the extreme of the permissible range of values for $\delta_{12}$; for example, the 10% critical value of chi-squared on 1 degree of freedom is 2.71, and we therefore reject statistical independence at the 5% level if $R(\hat{\delta}_{12}) > 2.71$ (Self & Liang, 1987). If statistical independence is rejected, an approximate 95% confidence interval for $\delta_{12}$ consists of all values of $\delta_{12}$ for which $R(\hat{\delta}_{12}) - R(\delta_{12})$ is less than 3.84, the 5% critical value of chi-squared on 1 degree of freedom.

In principle, the likelihood ratio approach could be used to test functional independence against general dependence, that is, a model in which $h_{12}(u)$ is specified by the more flexible interaction function [eqn. (3)]. However, the distribution theory for this nonregular multiparameter problem is not straightforward. For this reason, we have chosen to test directly the goodness of fit of the functional independence model, using methods described in the following section.

*Assessing goodness of fit*

To evaluate the spatial distributions of cells, we have used various spatial statistics. Many statistics have been proposed, none of which alone is sufficient to capture all the properties of spatial distributions. Our approach then has been to evaluate several complementary measures, rather than compute an exhaustive list of all known statistics.

The most familiar measure to visual neuroscientists is the regularity index (*RI*), the mean of the nearest-neighbor distances divided by the standard deviation of those distances (Wässle & Riemann, 1978). The higher this number, the more regular the distribution of cells. In practice, values above 2 typically indicate a regular distribution of cells since the theoretical *RI* for a completely random process is $[\pi/(4 - \pi)]^{0.5} = 1.913$; Cook (1996) provides tables giving thresholds for various cell densities and aspect ratios. The *RI*s for several simulated arrays are shown in Fig. 3.

We have also used $K$ functions (Ripley, 1976) to evaluate second-order properties of our spatial patterns. The DRP, more commonly used in studies of retinal mosaics, is simply the derivative of the $K$ function; both are second-moment methods. An advantage of $K$ for relatively small datasets is that it avoids the need for choosing an arbitrary bin-width. A counter-advantage of the DRP is that many people are more comfortable interpreting noncumulative functions (DRP) than cumulative functions ($K$). Estimates of $K$ functions and related spatial distributions were computed using the Splancs package in R (Rowlingson & Diggle, 1993; R Development Core Team, 2005).

The univariate estimated $K$ function is defined as

$$K(t) = \frac{|A|}{n(n-1)} \sum_{i=1}^{n} \sum_{j \neq i} w(i,j)^{-1} I(\|\mathbf{x}_i - \mathbf{x}_j\| \leq t). \qquad (6)$$

$I(\cdot)$ is the indicator function; it counts the number of cell pairs that are less than or equal to some distance $t$ apart from each other. The term $w(i,j)$ is the weighting factor to adjust for border corrections; it measures the fraction of the circumference of the circle centerd at $\mathbf{x}_i$ and with radius $\|\mathbf{x}_i - \mathbf{x}_j\|$ that is within the sampling window $A$. For a rectangular sampling window, an explicit formula can be written for $w$ (Diggle, 2002). Under the null hypothesis of CSR, the theoretical $K$ function is $K(t) = \pi t^2$.

The bivariate estimated $K$ function is similarly defined as

$$K_{12}(t) = \frac{|A|}{n_1 n_2} \sum_{i=1}^{n_1} \sum_{j=1}^{n_2} w(i,j)^{-1} I(\|\mathbf{x}_{1i} - \mathbf{x}_{2j}\| \leq t), \qquad (7)$$

where this time the weighting factor $w(i,j)$ is for the circle centered at $\mathbf{x}_{1i}$ and with radius $\|\mathbf{x}_{1i} - \mathbf{x}_{2j}\|$. For plotting purposes, we define $L(t) = (K(t)/\pi)^{0.5}$. Under CSR, the theoretical $L$ function is $L(t) = t$.

As a complement to $K$ functions, we also measure $G$ functions (Diggle, 2002). For the on-center cells

$$G_1(t) = \frac{1}{n_1} I(y_i \leq t), \qquad (8)$$

where $y_i$ is the distance of cell $i$ to its nearest neighbor of the same type. $G_2(t)$ is defined similarly for the off-center cells. Hence $G(t)$ is a cumulative version of the empirical nearest-neighbor distribution measuring the fraction of cells whose nearest neighbor is of distance less than $t$.

To evaluate the goodness of fit of our models, we use both qualitative and quantitative tests. Informally, if the distribution from the dataset falls within the 95% envelope of the simulations, we suggest there is a good fit. This visual evaluation can be

**Table 1.** *Summary of the spatial functions used in the paper*

| Term | Meaning |
|---|---|
| $K(t)$ | Expected number of cells within distance $t$ of an arbitrary cell, divided by cell density. This is the cumulative version of the density recovery profile (Rodieck, 1991). |
| $L_1(t)$, $L_2(t)$, $L_{1+2}(t)$ | Normalized version of $K(t)$, useful for plotting purposes since $L(t) = t$ if cells are randomly arranged. Subscripts denote whether on-center cells (1), off-center cells (2), or all cells (1 + 2) are being analyzed. |
| $L_{12}(t)$ | Bivariate version of the $L$ function, measuring the (normalized) expected number of on-center cells within a given distance of an arbitrary off-center cell (or *vice-versa*). This function is the (normalized) cumulative version of the density recovery profile from the cross-correlogram (Rodieck, 1991). |
| $G_1(t)$, $G_2(t)$ | Cumulative version of the nearest-neighbor distribution for on-center (1) or off-center (2) cells. |

quantified by computing Monte Carlo $p$ values. For each real and simulated dataset, we compute some measure $T$. The rank of $T$ (largest first) is converted to a $p$ value by dividing the rank by one plus the number of simulations (Barnard, 1963). The choice of test statistic $T$ depends on the context, as outlined below.

*Goodness of fit for G and K functions*

To assess the goodness of fit using the $G$ function, we use the test statistic

$$T^i = \int_0^{150\,\mu\text{m}} [G^i(t) - \overline{G^i}(t)]^2 \, \mathrm{d}t, \tag{9}$$

where $G^1$ is calculated from the data, $G^i$, $i = 2,\ldots,s + 1$ are calculated from $s$ simulations of the model and $\overline{G^i}(t) = (1/s)\sum_{j\neq i} G^j(t)$. The $T$ values are ranked as before to determine significance. The same approach can be used to assess the goodness of fit using the $K$ function. For example, the test statistic $T$ for evaluating $K_1$ is

$$T^i = \int_0^{150\,\mu\text{m}} (\sqrt{K_1^i(t)} - \sqrt{\overline{K_1^i}(t)})^2 \, \mathrm{d}t, \tag{10}$$

where

$$\overline{K_1^i}(t) = \frac{1}{s}\sum_{j\neq i} K_1^j(t).$$

Similar expressions can be determined to evaluate $K_2$ and $K_{1+2}$ (where 1 + 2 denotes that we consider all cells, irrespective of polarity). For convenience, the spatial functions are briefly summarised in Table 1.

*Voronoi-based measures*

Finally, the Voronoi domains of cells are computed to determine which cells are considered as neighbors of each other. Two cells are considered neighbors if they share an edge of a Voronoi polygon. For each mosaic, we rank the neighbors by distance and examine whether the nearest neighbors (or second-nearest, third-nearest) are of opposite type, or are of the same type. In addition, we measure the fraction of all Voronoi neighbors that are of the same type as a given cell. Cells that are defined as border cells (those whose Voronoi polygon intersects with the boundary of the tissue) are not included for measurement, but are eligible as nearest neighbors of nonborder cells. Border cells are also excluded from calculations of the regularity indices, which explains why our values are higher than those previously reported for the W81S1 dataset (Wässle et al., 1981*a*).

## Results

Following the methodology proposed by Diggle (1986), we first test for statistical dependence (Fig. 4). It can be seen that, as expected, statistical independence is rejected using the goodness-of-fit approach. In particular, the experimental $L_{12}$ function falls below the 95% envelope of the simulated data sets in the range 0–20 $\mu$m. Furthermore, the $T$ statistic [eqn. (1)] for the real dataset is larger than all of the simulations for map M623, and so we can reject statistical independence with $p = 0.001$. Likewise, statistical independence for W81S1 is rejected with $p = 0.006$. This confirms that we have sufficient points in each of our two datasets for further analysis.

*Estimation of interaction functions*

Fig. 5 summarizes the interaction functions that we calculated from our datasets. The nonparametric estimates (dotted lines) were estimated from the data using a piece-wise constant specification of $h(u)$. These are typically sigmoidal in nature: out to distances of around 30–50 $\mu$m, $h(u)$ is zero, reflecting the fact that no two cells of the same type are close to each other. Over the next 50–100 $\mu$m these estimates then rise typically to $h(u) = 1$ which indicates that

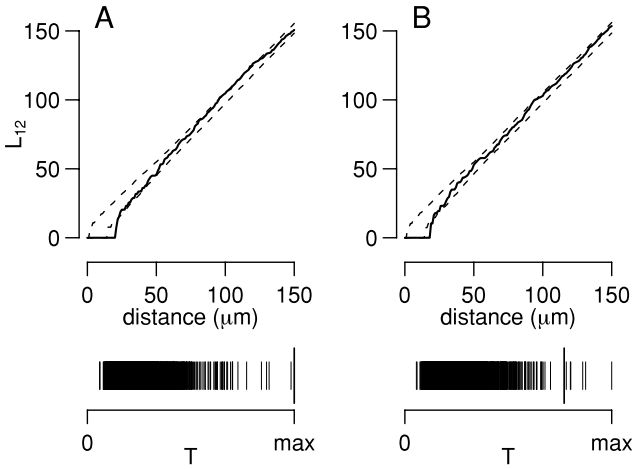


**Fig. 4.** Testing statistical independence of the two datasets. (A) Testing statistical independence of the M623 data set. The upper plot shows $L_{12}$ for the real data (thick black line) and the 95% envelope of $s = 999$ simulations created by toroidally shifting one of the datasets (dotted lines). Under statistical independence we would expect $L_{12}(t) = t$, i.e. for the data to fall along the leading diagonal. Underneath the plot is the $T$ score [eqn. (1)] for the real dataset (tall thick line), and for the 999 simulations (thin lines). Only the ranks of $T$, rather than absolute values, are important here. Statistical independence is rejected ($P = 0.001$). (B) Like A, for the W81S1 dataset. Again statistical independence is rejected ($P = 0.006$).

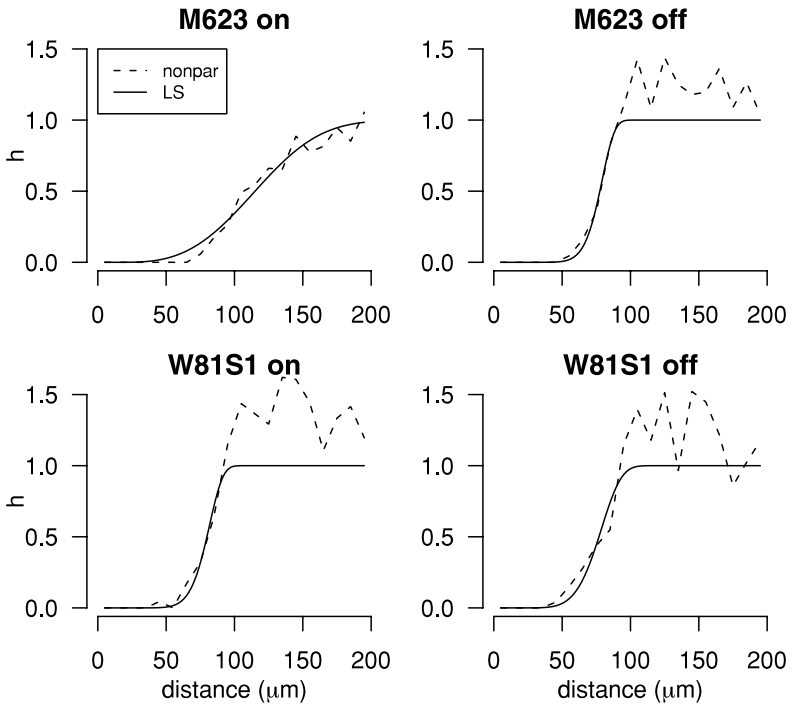


**Fig. 5.** Summary of the interaction functions that were computed from the fields. Dashed lines show the nonparametric estimates of the interaction function. The solid lines show the least-squares fit of the nonparametric estimates to our parametric interaction function. See Table 2 for parameter values.

the cell positions are independent of each other beyond a certain distance. With the exception of the M623 on-center cells, the nonparametric estimate of $h(u)$ peaks at a value greater than 1 at distances around 100–150 $\mu$m. This does not necessarily indicate a tendency for pairs of cells to aggregate at those distance, because the statistical fluctuations in the nonparametric estimates of $h(u)$ increase with $u$. We evaluate the uncertainty in the nonparametric estimation procedure in a later section, after the goodness-of-fit simulations have been introduced.

Given the sigmoidal-like nature of these nonparametric estimates of interaction functions, we then fit the parametric form of a sigmoidal-like curve [eqn. (3)] to each of these estimates. Fig. 5 shows the corresponding fits for each dataset, and the parameters found are listed in Table 2. In general, there is good agreement between the nonparametric estimates and the corresponding parametric fits; the two curves for each field obviously differ at distances greater than around 100 $\mu$m, since the parametric curve by definition has a maximal value of $h(u) = 1$.

### *Testing statistical independence versus functional dependence*

Using the estimates of $\alpha$ and $\phi$ for each retinal mosaic, we then used the likelihood ratio test to compare the likelihood of the form of interaction between on- and off-center cells ($\delta_{12}$) under the two hypotheses of statistical independence and functional independence

Under the null hypothesis of statistical independence, $\delta_{12} = 0$, and using the univariate parameter fits, the log likelihood was calculated (Diggle et al., 2005). Likewise, the log-likelihood was calculated under the hypothesis of functional independence, in which $h_{12}$ took the form of eqn. (2) with $\delta_{12}$ varying from 0 to either 18 or 20 $\mu$m in 1-$\mu$m increments. By definition, $\delta_{12}$ could not be greater than the smallest observed distance between cells of opposite type, namely 20.0 $\mu$m for M623 and 18.1 $\mu$m for W81S1. For each value of $\delta_{12}$, we calculated twice the Monte-Carlo log-likelihood ratio, $R(\delta_{12})$, as shown in Fig. 6. From these profiles, we determined the maximum-likelihood estimates of $\hat{\delta}_{12}$ (Table 2) as the values corresponding to the maximal values of $R(\delta_{12})$. Furthermore, we could then compute the 95% confidence intervals for the estimate of $\delta_{12}$, namely 9–18 $\mu$m for W81S1 and 13–20 $\mu$m for M623 (horizontal arrow in Fig. 6). For both maps, our lower bound estimate of soma diameter, 15 $\mu$m, is within these confidence intervals. We use the upper end of the confidence interval as a point estimate because, for simple inhibitory models this is generally the maximum-likelihood estimate. The values of $R(\hat{\delta}_{12})$ are compared with their reference distribution under the

**Table 2.** *Summary of parameter estimates for the univariate functions $h_{11}(u)$, $h_{22}(u)$ and the bivariate function $h_{12}(u)$*[a]

| | $\phi$($\mu$m) | $\alpha$ | $\delta_{12}$ ($\mu$m) |
|---|---|---|---|
| W81S1 | | | |
| $h_{11}(u)$ | 67.94 | 7.81 | |
| $h_{22}(u)$ | 66.27 | 5.40 | |
| $h_{12}(u)$ | | | 18 |
| M623 | | | |
| $h_{11}(u)$ | 112.79 | 3.05 | |
| $h_{22}(u)$ | 65.46 | 8.11 | |
| $h_{12}(u)$ | | | 20 |

[a]For the univariate fits, $\alpha$ and $\phi$ are least-square estimates (assuming $\delta$ was fixed at 15 $\mu$m). See also Fig. 5 for the interaction functions using these parameter estimates. The final column gives the maximum likelihood estimate of $\delta_{12}$ assuming that the interaction between types is simple inhibition [eqn. (2)]. See Fig. 6 and the section on Testing statistical independence vs. functional dependence for how $\delta_{12}$ was determined for each field.

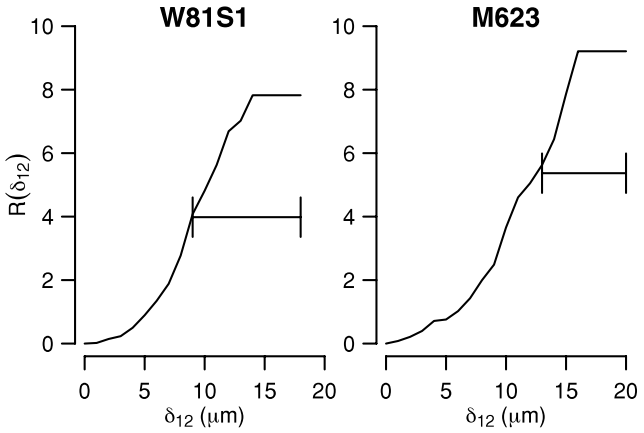


**Fig. 6.** Log-likelihood profile plot comparing the null hypothesis of statistical independence against functional independence. For values of $\delta_{12}$ greater than the smallest observed distance between cells of different types, the log likelihood ratio is negative infinity. Horizontal bar denote 95% confidence intervals for the value of $\delta_{12}$ under functional independence. Since the confidence intervals exclude zero, the null hypothesis of statistical independence is rejected against the alternative of functional independence. In both cases, the maximum likelihood estimate is at the upper end of the confidence interval (18 $\mu$m for W81S1 and 20 $\mu$m for M623).

null hypothesis of statistical independence, as described in a previous section. In both cases, statistical independence was rejected ($p = 0.003$ for W81S1 and $p = 0.001$ for M623).

In principle, the likelihood ratio test can also be applied to compare the likelihood when $h_{12}(u)$ is a simple inhibition function versus when it can take a wider range of shapes through our parameterization of $h(u)$ [eqn. (3)]. However, the distribution theory is more complex than testing functional independence against statistical independence, since three parameters need to be optimized, rather than one, and all three are subject to boundary constraints. Exploration of parameter space showed that no better likelihoods were computed when $h_{12}(u)$ took the form of eqn. (3) rather than when $h_{12}(u)$ was fixed to be the simple inhibition function [eqn. (2)]. In this case therefore, the likelihood ratio was not computed, as it was deemed to be too small to show any difference between the two models. Hence, we conclude that the general bivariate model does not fit the data any better than the model assuming functional independence.

*Goodness of fit for the interaction functions*

As a complement to the likelihood ratio testing, we tested whether our parametric interaction functions capture the spatial properties of the retinal mosaics. We simulated fields using the bivariate PIPP model (see Methods). An example of each simulated field can be seen in Fig. 2, beneath the corresponding real field. Visually, the real and simulated fields appear quite similar in their distributions.

To quantitatively evaluate the goodness of the fit of the model to each dataset, we ran 999 simulations for each field, and compared spatial distributions for the real field and the simulated fields. Results for the two fields are shown in Figs. 7 and 8. In these figures, solid lines show the $L$ and $G$ functions for the real data, whereas dotted lines indicate the 95% envelope from the simulations. ($L$ and $G$ are summarized in Table 1). In general (but see below for exceptions), we find that the qualitative nature of the fits of the model to the data is encouraging: for the $L$ and $G$ functions, the real curve lies within the envelope formed by the simulations. Occasionally, the real curve dips out of the range of the simulations, but this tends to happen at larger distances, where the estimates are less accurate anyway. This in general accounts for the low $p$ values.

$L(t)$ is derived from the $K$ function, which measures the expected number of cells within a distance $t$ of a cell. The univariate $L$ functions ($L_1$ and $L_2$) indicate that no two cells of the same type are closer than around 50 $\mu$m. Furthermore, since $L(t) \approx t$ once $t$ approaches 150 $\mu$m, this indicates interactions are fairly short-range. When all cells are considered irrespective of type, the $L_{1+2}$ curves indicate that there are no interactions beyond about 20 $\mu$m. Likewise, the bivariate $L_{12}$ function shows interactions between the two types that we believe are limited to preventing somal overlap. Importantly, there is good agreement (both visually using the simulation envelope and quantitatively using the $p$ values) between model and data for $L_{12}$, strengthening our conclusion of functional independence between the on- and off-center arrays. Although some $p$ values are quite small, in general the 95% simulation envelopes mostly agree with the data. The major exception for the fits to the $L$ functions is $L_1$ for M623: the model fields are much less regular than M623 on. We believe this to be caused by poor estimation of $h(u)$ for this field, which also affects $G_1$ and the regularity indices for this field. Comparing the interaction functions (Fig. 5), the $h(u)$ function is much broader for M623 on-center field than for the other three fields, and this reduces the regularity of the simulated M623 on fields.

The $G$ functions are cumulative nearest-neighbor distributions, and are typical of that expected for regular distributions of cells. The $G$ distributions are further quantified in the regularity indices, showing that either the on- or off-center map alone is more regular than the mosaic of all beta RGCs. As mentioned above, the main problem is with the $G$ function for M623 on-center field, where the simulations are less regular than the real field. However the $G$ functions for W81S1 show a minor discrepancy around $G = 0.5$, which we think represents minor fluctuations responsible for the low $p$ values.

Finally, we have used the Voronoi tessellation to define which cells are nearest neighbors (and second-nearest, and so on) of each other, and then to count the fraction of nearest neighbors that were of opposite sign (Zhan & Troy, 2000). These measures show that nearly all nearest neighbors are of the opposite type, as reported before (Wässle et al., 1981*a*).

In summary, the model produces generally good fits to the data, albeit with some discrepancies. The main point for using the modelling was to test the hypothesis of functional independence, rather than to get the best fits between model and data. Most of the discrepancies are due to the poor fit of the model to the M623 on data. If different parameters are selected (by hand) for the M623 on-center field, fits for $L_1$ and $G_1$ improve (Fig. 9). However, the advantage of the method presented here is that no hand-tuning of parameter estimates is required.

*Evaluating the uncertainty in nonparametric estimation of $h(\cdot)$*

Our goodness-of-fit simulations indicate that our parametric form of homotypic interaction functions [eqn. (3)] captures the spatial interactions among on- or off-center cells. One possible concern using this parametric form is that it cannot represent any interactions where $h(u) > 1$, and yet three of the four nonparametric estimates of $h(u)$ show rises above 1.0 for distances greater than around 100 $\mu$m (Fig. 5). We consider now whether these rises

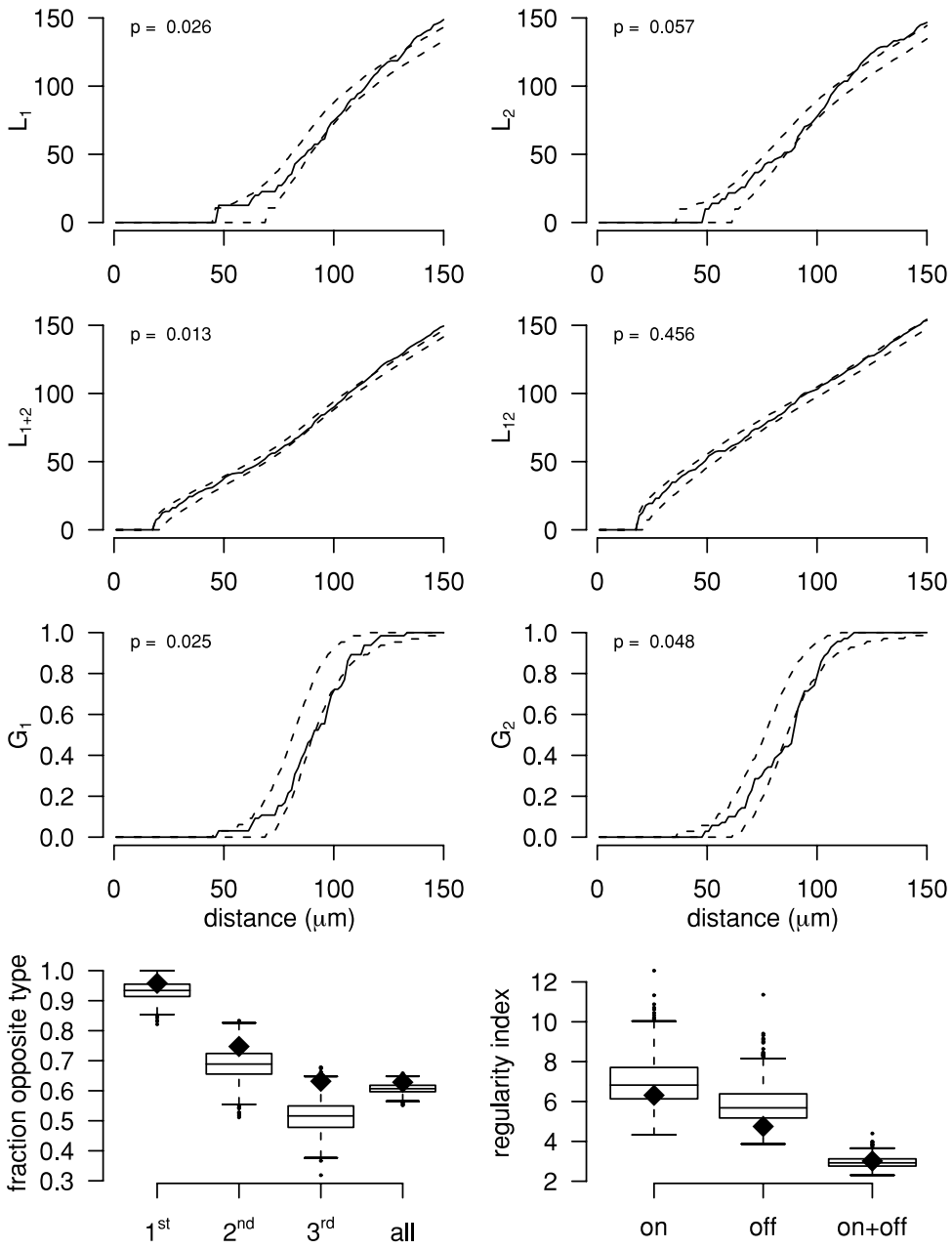


**Fig. 7.** Goodness-of-fit testing for W81S1 field with the bivariate PIPP model, using parameters listed in Table 2. Univariate $L$ functions are plotted for on-center (1), off-center (2), all cells irrespective of center (1 + 2), and the bivariate $L_{12}$ function. $G$ function for both on- and off-center cells are also shown. For $L$ and $G$ functions, the solid line is the observed value, and dotted lines indicate the 95% simulation envelope. P values denote the goodness of fit. Bottom left: fraction of nearest-neighbors that are of opposite type. Diamonds indicate values from real maps, and box plots indicate the range of values from the simulations. (Each rectangle marks the 1st, 2nd, and 3rd quartile; whiskers are drawn out to 1.5 times the interquartile range, with small dots indicating individual values outside that range.) Bottom right: regularity indices for real and simulated maps in same format.

above 1.0 might be explainable simply by statistical uncertainty in the nonparametric estimation procedure. To test this, for each field, we estimated $h(u)$ from 99 of the simulated fields summarized in Figs. 7 and 8. If the nonparametric estimation procedure is working reliably, the nonparametric estimates would be similar to the known parametric shape of $h(u)$ that we used for each simulation. The results are shown in Fig. 10. We find that even when $h(u)$ is known to be constrained within [0.0, 1.0], the nonparametric estimation procedure often estimates $h(u) > 1.0$. We therefore believe that the discrepancies between nonparametric and parametric estimates of $h(u)$ in Fig. 5 are simply due to uncertainties in the nonparametric estimation, and therefore do not invalidate a model with $h(u)$ limited to the range [0.0, 1.0].

## Discussion

We have demonstrated that the mosaics of on- and off-center beta RGCs are broadly consistent with the functional independence hypothesis. We have argued that functional independence, rather than statistical independence, is the scientifically natural null

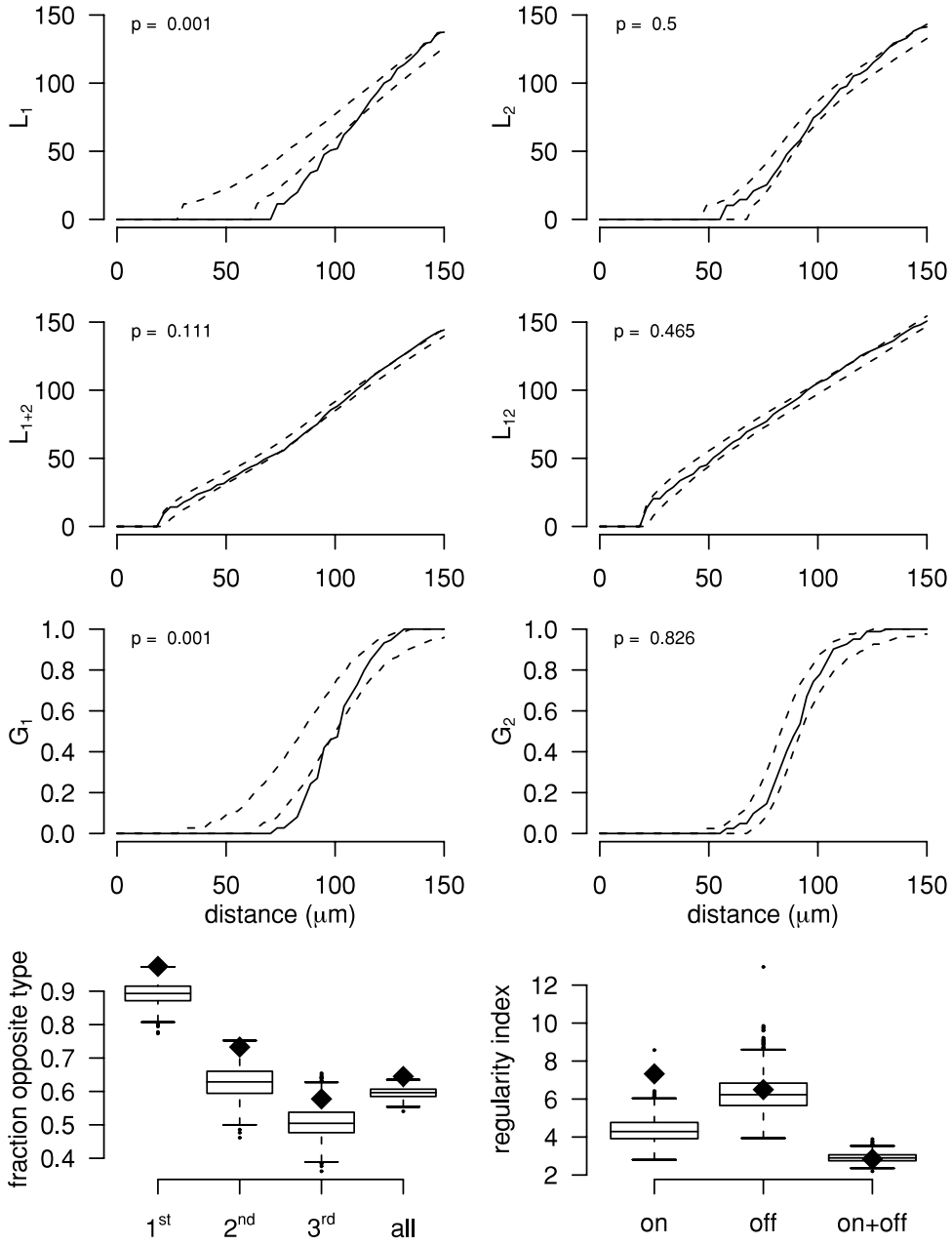


**Fig. 8.** Goodness-of-fit testing for M623 field with the bivariate PIPP model, using parameters listed in Table 2. Plotting conventions are the same as in Fig. 7.

hypothesis and have used a likelihood ratio method to estimate the functional independence parameter $\delta_{12}$, having first confirmed that the data do contain sufficient information formally to reject the hypothesis of statistical independence. For both datasets, the confidence interval for $\delta_{12}$ includes the value 15 $\mu$m, consistent with our estimate of the lower bound for soma diameter. We have used a variety of *ad hoc* measures to evaluate the quality of our model fits to the two datasets. In some cases, these reveal statistically significant discrepancies between data and model. However, our overall conclusion from graphical comparison between empirical summaries of data and model (Figs. 2, 7, and 8) is that the bivariate functional independence model gives a good approximate description of the spatial structure of the RGC mosaics. Our conclusion of functional independence between on-and off-center RGCs is in general agreement with previous observations suggesting that spatial dependencies between pairs of cell types are rare (Kouyama & Marshak, 1997; Rockhill et al., 2000; Ahnelt et al., 2000).

Our results elaborate on an earlier model which suggested some spatial dependencies between the on- and off-center beta RGCs (Zhan & Troy, 2000). In this model, two triangular lattices of cells were jittered to create the final pattern of RGCs, under two constraints: first, the two lattices had to be displaced from each other by a fixed vector, and second, somal overlap was prohibited. The first constraint does not embody any biological principle, but is required as a consequence of starting with regular arrays. By contrast, our current model takes a more developmental approach

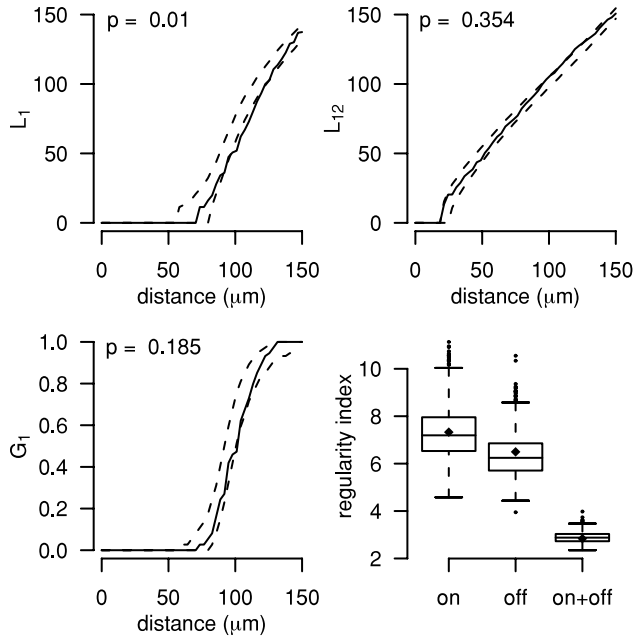


**Fig. 9.** Goodness-of-fit testing for M623 field, using different parameters for M623 on ($\phi = 75$ $\mu$m, $\alpha = 10.0$) with all other parameters as in Table 2. (No attempt was made to optimize the parameters.) Compared with Fig. 8, the fit between model and data for $L_1$ and $G_1$ are better (although $L_1$ still shows discrepancies around 100–120 $\mu$m) without affecting the cross-correlation curve ($L_{12}$).

by gradually rearranging cell positions from random starting points, and so does not require such a constraint. The second constraint, preventing somal overlap, is common to both models, and we believe is the only constraint acting between cells of different type. Our current model also provides a more parsimonious explanation for mosaic formation than a previous model where it was suggested that lateral inhibition of cell fate followed by cell death

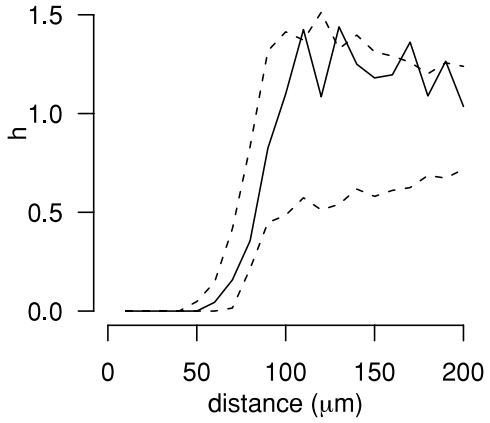


**Fig. 10.** Evaluating the statistical uncertainty in the nonparametric estimation procedure. Solid line shows the nonparametric estimate of $h(u)$ for M623 off-center cells (repeated from Fig. 5). Dashed lines show the 95% envelope from 99 simulations of the M623 off-center cells summarized in Fig. 8. Simulations from the three other fields produced similar simulation envelopes.

could generate the beta RGC mosaics (Eglen & Willshaw, 2002). Finally, a recent model investigating the role of RGC mosaics upon cortical orientation selectivity assumed statistical independence between on- and off-center cells (Ringach, 2004). Our results suggest that more realistic mosaics would be created by including the constraint that somas should not overlap.

### *Mechanisms of pattern formation*

Our current model suggests that beta retinal ganglion cells are formed by mostly homotypic interactions: the extent of the heterotypic interactions (up to 20 $\mu$m) is much smaller than the range of homotypic interactions (50–100 $\mu$m). However, our model does not suggest what biological mechanisms drive those interactions. Previous work has shown that during development, RGCs move laterally within the ganglion cell layer (Reese & Galli-Resta, 2002) and theoretical models suggest that this movement is sufficient to drive mosaic formation (Eglen et al., 2000). We therefore suggest that lateral movement of cell bodies is one mechanism by which cells respond to the homotypic constraints upon cell positioning. Our model suggests that the only heterotypic constraint is that imposed naturally by preventing somas from occupying the same space in the ganglion cell layer. Such a constraint may not apply in the area centralis where cells are displaced vertically within the ganglion cell layer (Kolb & Nelson, 1984).

However, although our current model suggests that there are limited heterotypic constraints upon cell positioning, our model cannot discriminate between alternative mechanisms (reviewed in Cook & Chalupa, 2000) that could potentially underly the homotypic constraints. This is because the homotypic interactions are specified only in terms of the probabilities of finding cells at a given distance from each other, without reference to how the nervous system might determine those probabilities. However, our model can predict the range over which such interactions may exist. With the exception of the M623 on-center field, the homotyptic interaction functions have reached 1.0 by around 100 $\mu$m (see Fig. 5), and therefore suggests that homotypic interactions are likely to be fairly local, around 100 $\mu$m or less.

Further elucidation of the mechanisms underlying mosaic formation in the beta RGCs awaits more experimental data. The availability of a neurochemical marker to distinguish on-center versus off-center cells would be invaluable to allow the collection of more experimental maps, especially if the marker reliably identifies cell types early enough during development. To date, such a marker has remained elusive, but previously, cytochrome oxidase staining was used to label populations of RGCs, on the basis that off-center cells were more heavily stained (Kageyama & Wong-Riley, 1984). However, this technique worked better for alpha than for beta RGCs, and although we believe similar developmental mechanisms might apply for alpha and beta RGCs, alpha cells are of much lower density and so are likely to show nonstationarity within a field of sufficient sample size (Wässle et al., 1981*b*). This nonstationarity is caused by the dependence of eccentricity on cell density. Nonstationary data can be analyzed and modelled in a similar fashion to the methods presented here, but it requires the form of nonstationarity to be quantified so that it can be taken into account.

### *Modeling considerations*

The bivariate PIPP model is similar in spirit to the minimal distance, or $d_{min}$, model, which has previously been used to

replicate several different retinal mosaics (Galli-Resta et al., 1997, 1999; Cellerino et al., 2000; Raven et al., 2003). In this model, cells are positioned serially into the mosaic at random, subject to the constraint that the distance to the nearest-neighboring cell is greater than some minimal distance, $d_{min}$. However, there are two main differences between the two models.

First, if the interaction function for a univariate PIPP model takes the form of simple inhibition with $\delta$ in eqn. (2) set to $d_{min}$, the PIPP model can emulate the $d_{min}$ model behavior. However, the value of $d_{min}$ is usually drawn from a Normal distribution and thus varies from cell to cell. A randomly varying inhibition distance in the $d_{min}$ model is analogous to (albeit formally different from) allowing a non-simple inhibitory $h(u)$ in the PIPP model.

The second difference between the two models is an implementation detail. The $d_{min}$ model is usually implemented in a sequential fashion: cells are added to the simulation serially until enough cells have been positioned in the array. This means that when the $d_{min}$ parameter is large enough, later-positioned cells have a much harder time being positioned in the array than earlier-positioned cells. The $d_{min}$ model therefore cannot generate patterns that are highly regular; the typical packing density is about 0.55, which is quite low compared to the theoretical limit of 0.91 for cells arranged in a triangular lattice (Tanemura, 1979; Diggle, 2002). By contrast, the PIPP model is implemented using the birth and death algorithm, whereby a given cell is repositioned many times, and no one cell has a particular advantage from being placed "earlier" than other cells. It is likely that the PIPP model is closer to matching the biological reality than the $d_{min}$ model, since cells that arrive earlier in the destination layer of the retina probably adjust their position in response to later arriving cells. The $d_{min}$ model can be implemented using a birth and death algorithm and can replicate the spatial pattern of beta RGCs (data not shown). This claim of biological plausibility for the PIPP model assumes that lateral migration of RGCs is the dominant mechanism underlying the homotypic interactions. However, as mentioned in the previous section, our PIPP model makes no claim as to whether RGCs undergo lateral migration, rather than, say, cell death, to form regular mosaics. In this sense, our PIPP model is like the $d_{min}$ model which shows that exclusion zone models can generate mosaic patterns, but cannot show how the exclusion zone is generated (Galli-Resta et al., 1997). To address this question theoretically, models must be built that are based directly upon particular developmental mechanisms.

Our approach to modeling retinal cell mosaics is novel, in that it proposes using an initial nonparametric estimation procedure for the interaction function $h(u)$ (Baddeley & Turner, 2000), which can then be used to suggest a suitable parametric form, and to estimate model parameters routinely using a simple nonlinear least-squares method. The fitted parametric model can then be used to simulate fields similar in their spatial structure to the real mosaics. Once the parametric form of $h(u)$ is chosen, this method is automatic and faster than exhaustive searches of parameter space to find good fits between model and data (Raven et al., 2003). However, the method is not yet robust since it could not replicate well one of our four fields (M623 on-center). Some hand-tuning of parameters to generate better fits may always be possible.

*Summary*

In conclusion, our results suggest that the on- and off-center beta RGCs are positioned functionally independently of each other, subject only to the constraint that somas cannot overlap. This suggests that beta RGCs are destined to become on- or off-center at an early stage of development, and that competitive environmental interactions between the cells to define their responsiveness to light is unlikely. Such a view is supported by findings that show alpha RGCs in ferret are able to recognize and make dendritic contact with neighboring cells of the same polarity, even at very early stages in development, prior to visual responses (Lohmann & Wong, 2001). Furthermore, the relative numbers of on- versus off-center alpha RGCs can vary with retinal eccentricity, in support of the two systems working independently (Peichl, 1989). Given also physiological differences between on- and off-center RGCs (Chichilnisky & Kalmar, 2002), it is more likely that the two cell types develop independently rather than by relying on heterotypic developmental interactions.

## Acknowledgments

Thanks to Dr. Rolf Turner with advice on nonparametric estimates of interaction functions. This work was supported by a Wellcome Trust fellowship (S.J.E.), a Senior Fellowship (P.J.D.) from the UK Engineering and Physical Sciences Research Council (Grant number GR/S48059/01), and a NIH grant (J.B.T.; R01 EY06669).

## References

Ahnelt, P.K., Fernändez, E., Martinez, O., Bolea, J.A. & Kübber-Heiss, A. (2000). Irregular S-cone mosaics in felid retinas. Spatial interaction with axonless horizontal cells, revealed by cross correlation. *Journal of the Optical Society of America A* **17**, 580–588.

Baddeley, A. & Turner, R. (2000). Practical maximum pseudolikelihood for spatial point patterns. *Australian and New Zealand Journal of Statistics* **42**, 283–322.

Baddeley, A. & Turner, R. (2005). Spatstat: An R package for analyzing spatial point patterns. *Journal of Statistical Software* **12**, 1–42.

Barnard, G.A. (1963). Contribution to the discussion of Professor Bartlett's paper. *Journal of the Royal Statistical Society B* **25**, 294.

Besag, J.E. (1978). Some methods of statistical analysis for spatial data. *Bulletin of the International Statistical Institute* **47 (Book 2)**, 77–92.

Bodnarenko, S.R. & Chalupa, L.M. (1993). Stratification of ON and OFF ganglion cell dendrites depends on glutamate-mediated afferent activity in the developing retina. *Nature* **364**, 144–146.

Boycott, B.B. & Wässle, H. (1974). The morphological types of ganglion cells of the domestic cat's retina. *Journal of Physiology* **240**, 397–419.

Cellerino, A., Novelli, E. & Galli-Resta, L. (2000). Retinal ganglion cells with NADPH-diaphorase activity in the chick form a regular mosaic with a strong dorsoventral asymmetry that can be modelled by a minimal spacing rule. *European Journal of Neuroscience* **12**, 613–620.

Chichilnisky, E.J. & Kalmar, R.S. (2002). Functional asymmetries in on and off ganglion cells of primate retina. *Journal of Neuroscience* **22**, 2737–2747.

Cook, J.E. (1996). Spatial properties of retinal mosaics: An empirical evaluation of some existing measures. *Visual Neuroscience* **13**, 15–30.

Cook, J.E. & Chalupa, L.M. (2000). Retinal mosaics: New insights into an old concept. *Trends in Neuroscience* **23**, 26–34.

Cook, J.E. & Podugolnikova, T.A. (2001). Evidence for spatial regularity among retinal ganglion cells that project to the accessory optic system in a frog, a reptile, a bird, and a mammal. *Visual Neuroscience* **18**, 289–297.

Diggle, P.J. (1986). Displaced amacrine cells in the retina of a rabbit: Analysis of a bivariate spatial point pattern. *Journal of Neuroscience Methods* **18**, 115–125.

Diggle, P.J. (2002). *Statistical Analysis of Spatial Point Patterns*, second edition. London: Edward Arnold.

Diggle, P.J., Eglen, S.J. & Troy, J.B. (2005). Modelling the bivariate spatial distribution of amacrine cells. In *Case Studies in Spatial Point Process Modelling*, ed. Baddeley, A., Gregori, P., Mateu, J., Stoica, R. & Stoyan, D. Lecture Notes in Statistics 185. Springer (in press).

Eglen, S.J. & Willshaw, D.J. (2002). Influence of cell fate mechanisms upon retinal mosaic formation: A modelling study. *Development* **129**, 5399–5408.

Eglen, S.J., van Ooyen, A. & Willshaw, D.J. (2000). Lateral cell movement driven by dendritic interactions is sufficient to form retinal mosaics. *Network: Computation in Neural Systems* **11**, 103–118.

Eglen, S.J., Raven, M.A., Tamrazian, E. & Reese, B.E. (2003). Dopaminergic amacrine cells in the inner nuclear layer and ganglion cell layer comprise a single functional retinal mosaic. *Journal of Comparative Neurology* **466**, 343–355.

Enroth-Cugell, C. & Robson, J.G. (1966). The contrast sensitivity of retinal ganglion cells of the cat. *Journal of Physiology* **187**, 517–522.

Famiglietti, Jr., E.V. & Kolb, H. (1976). Structural basis for ON- and OFF-center responses in retinal ganglion cells. *Science* **194**, 193–195.

Galli-Resta, L., Novelli, E., Kryger, Z., Jacobs, G.H. & Reese, B.E. (1999). Modelling the mosaic organization of rod and cone photoreceptors with a minimal-spacing rule. *European Journal of Neuroscience* **11**, 1461–1469.

Galli-Resta, L., Resta, G., Tan, S.-S. & Reese, B.E. (1997). Mosaics of Islet-1-expressing amacrine cells assembled by short-range cellular interactions. *Journal of Neuroscience* **17**, 7831–7838.

Heikkinen, J. & Penttinen, A. (1999). Bayesian smoothing in the estimation of the pair potential function of Gibbs point processes. *Bernoulli* **5**, 1119–1136.

Kageyama, G.H. & Wong-Riley, M.T. (1984). The histochemical localization of cytochrome oxidase in the retina and lateral geniculate nucleus of the ferret, cat, and monkey, with particular reference to retinal mosaics and on/off-center visual channels. *Journal of Neuroscience* **4**, 2445–2459.

Kolb, H. & Nelson, R. (1984). Neural architecture of the cat retina. *Progress in Retinal Research* **3**, 21–60.

Kouyama, N. & Marshak, D.W. (1997). The topographical relationship between two neuronal mosaics in the short wavelength-sensitive system of the primate retina. *Visual Neuroscience* **14**, 159–167.

Kuffler, S.W. (1953). Discharge patterns and functional organisation of mammalian retina. *Journal of Neurophysiology* **16**, 37–68.

Lohmann, C. & Wong, R.O.L. (2001). Cell-type specific dendritic contacts between retinal ganglion cells during development. *Journal of Neurobiology* **48**, 150–162.

Lotwick, H.W. & Silverman, B.W. (1982). Methods for analysing spatial processes of several types of points. *Journal of the Royal Statistical Society B* **44**, 406–413.

Nelson, R., Famiglietti, Jr., E.V. & Kolb, H. (1978). Intracellular staining reveals different levels of stratification for on- and off-center ganglion cells in cat retina. *Journal of Neurophysiology* **41**, 472–483.

Peichl, L. (1989). Alpha and delta ganglion cells in the rat retina. *Journal of Comparative Neurology* **286**, 120–139.

R Development Core Team (2005). *R: A Language and Environment for Statistical Computing*. R Foundation for Statistical Computing, Vienna, Austria. ISBN 3-900051-07-0.

Raven, M.A., Eglen, S.J., Ohab, J.J. & Reese, B.E. (2003). Determinants of the exclusion zone in dopaminergic amacrine cell mosaics. *Journal of Comparative Neurology* **461**, 123–136.

Reese, B.E. & Galli-Resta, L. (2002). The role of tangential dispersion in retinal mosaic formation. *Progress in Retinal and Eye Research* **21**, 153–168.

Ringach, D.L. (2004). Haphazard wiring of simple receptive fields and orientation columns in visual cortex. *Journal of Neurophysiology* **92**, 468–476.

Ripley, B.D. (1976). The second-order analysis of stationary point processes. *Journal of Applied Probability* **13**, 255–266.

Ripley, B.D. (1977). Modelling spatial patterns (with discussion). *Journal of the Royal Statistical Society B* **39**, 172–212.

Ripley, B.D. (1979). AS137 Simulating spatial patterns. *Applied Statistics* **28**, 109–112.

Rockhill, R.L., Euler, T. & Masland, R.H. (2000). Spatial order within but not between types of retinal neurons. *Proceedings of the National Academy of Sciences of the U.S.A.* **97**, 2303–2307.

Rodieck, R.W. (1991). The density recovery profile: A method for the analysis of points in the plane applicable to retinal studies. *Visual Neuroscience* **6**, 95–111.

Rodieck, R.W. & Marshak, D.W. (1992). Spatial density and distribution of choline acetyltransferase immunoreactive cells in human, macaque and baboon retinas. *Journal of Comparative Neurology* **321**, 46–64.

Rowlingson, B.S. & Diggle, P.J. (1993). Splancs: Spatial point pattern analysis code in S-Plus. *Computers and Geosciences* **19**, 627–655.

Self, S.G. & Liang, K.-Y. (1987). Asymptotic properties of maximum likelihood estimators and likelihood ratio tests under nonstandard conditions. *Journal of the American Statistical Association* **82**, 605–610.

Stein, J.J., Johnson, S.A. & Berson, D.M. (1996). Distribution and coverage of beta-cells in the cat retina. *Journal of Comparative Neurology* **372**, 597–617.

Tanemura, M. (1979). On random complete packing by discs. *Annals of the Institute of Statistical Mathematics* **31**, 351–365.

Wässle, H. & Riemann, H.J. (1978). The mosaic of nerve cells in the mammalian retina. *Proceedings of the Royal Society B* (London) **200**, 441–461.

Wässle, H., Boycott, B.B. & Illing, R.B. (1981*a*). Morphology and mosaic of on-beta and off-beta cells in the cat retina and some functional considerations. *Proceedings of the Royal Society B* (London) **212**, 177–195.

Wässle, H., Peichl, L. & Boycott, B.B. (1981*b*). Morphology and topography of on-alpha and off-alpha cells in the cat retina. *Proceedings of the Royal Society B* (London) **212**, 157–175.

Zhan, X.J. (1996). *Properties of ON- and OFF-center beta cell somatic and dendritic mosaics in cat retina*. Ph.D. Thesis, Northwestern University, Evanston, Illinois.

Zhan, X.J. & Troy, J.B. (2000). Modeling cat retinal beta-cell arrays. *Visual Neuroscience* **17**, 23–39.